Journal peer review information: *Nature Communications* thanks Vincenzo De Luca, Thierry Delatte and the other anonymous reviewers for their contribution to the peer review of this work. Peer reviewer reports are available.

Cytosolic lipid droplets as engineered organelles for production and accumulation of terpenoid biomaterials in leaves

Radin Sadre[1,2,3]*, Peiyen Kuo[2], Jiaxing Chen[2], Yang Yang[2,3,4], Aparajita Banerjee[2,3], Christoph Benning[2,3,4,5] and Bjoern Hamberger[2,3]*

[1]Department of Horticulture, Michigan State University, East Lansing, Michigan 48824

[2]Department of Biochemistry and Molecular Biology, Michigan State University, East Lansing, Michigan 48824

[3]Great Lakes Bioenergy Research Center, Michigan State University, East Lansing, Michigan 48824

[4]MSU-DOE Plant Research Laboratory, Michigan State University, East Lansing, Michigan 48824

[5]Department of Plant Biology, Michigan State University, East Lansing, Michigan 48824

*Address correspondence to sadre@msu.edu, hamberge@msu.edu

ABSTRACT

Cytosolic lipid droplets are endoplasmic reticulum-derived organelles typically found in seeds as reservoirs for physiological energy and carbon to fuel germination. Here, we report synthetic biology approaches to co-produce high-value sesqui- or diterpenoids together with lipid droplets in plant leaves. The formation of cytosolic lipid droplets is enhanced in the transient *Nicotiana benthamiana* system through ectopic production of WRINKLED1, a key regulator of plastid fatty acid biosynthesis, and a microalgal lipid droplet surface protein. Engineering of the pathways providing the universal C5-building blocks for terpenoids and installation of terpenoid biosynthetic pathways through direction of the enzymes to native and non-native compartments boost the production of target terpenoids. We show that anchoring of distinct biosynthetic steps onto the surface of lipid droplets leads to efficient production of terpenoid scaffolds and functionalized terpenoids. The co-produced lipid droplets "trap" the terpenoids in the cells.

INTRODUCTION

Cytosolic lipid droplets are dynamic organelles typically found in seeds as reservoirs for physiological energy and carbon in form of triacylglycerol (oil) to fuel germination. They are derived from the endoplasmic reticulum (ER) where newly synthesized triacylglycerol accumulates in lens-like structures between the leaflets of the membrane bilayer[1]. After growing in size, the structures bud off from the outer membrane of the ER. A mature lipid droplet is composed of a hydrophobic core of triacylglycerol surrounded by a phospholipid monolayer and coated with lipid droplet associated proteins involved in the biogenesis and function of the organelle. In seeds, oleosin proteins coat and stabilize small lipid droplets preventing coalescence. These proteins contain surface-oriented

amphipathic N- and C-termini essential to efficiently emulsify lipids and a conserved hydrophobic central domain anchoring the oleosins onto the surface of lipid droplets[2].

Due to the potential economical relevance of plant lipids as renewable resource for the production of high-density biofuels, strategies have been established to enhance the accumulation of triacylglycerol in vegetative tissues of high-biomass yielding crops[3-5]. A primary target for increasing lipid production has been engineering the expression of *WRINKLED1*. The gene encodes a member of the AP2/EREBP family of transcription factors and master regulator of fatty acid biosynthesis in seeds[6,7]. Its ectopic production in vegetative tissues promotes fatty acid synthesis in the plastids and, indirectly, triacylglycerol accumulation in lipid droplets[4,8-10]. Yields of triacylglycerol were further increased by removal of an intrinsically disordered region of *Arabidopsis thaliana* WRINKLED1 (*At*WRI1$^{1-397}$) increasing the protein's stability[11] and through engineered co-production of WRINKLED1 with ectopic lipid biosynthesis enzymes and a plant lipid droplet associated protein[3,9].

Plant-derived terpenoids have a wide range of industrial uses such as specialty fuels, agrochemicals, fragrances, nutraceuticals and pharmaceuticals. The limited economic sustainability of formal (petro-) chemical synthesis, or extraction and purification from the native plant source has motivated biotechnological approaches to produce industrially relevant terpenoids[12-15]. Plants accumulating high levels of terpenoids have evolved specialized anatomical features for their biosynthesis and storage including laticifer cells, resin ducts or cavities, and glandular trichomes[16]. The recently reported accumulation of terpenoids together with neutral lipids in lipid droplets in the outer root cork cells of *Plectranthus barbatus* (synonym *Coleus forskohlii*), was suggested as a mechanism to enrich and sequester the bioactive defense compounds intracellularly[17]. The co-occurrence of lipids and terpenoids invites opportunities for biotechnology to engineer the high-yield production and storage of terpenoids in vegetative tissues of lipid droplet-accumulating biomass crops. In plants, the C5-building blocks of terpenoids, dimethylallyl diphosphate (DMADP) and isopentenyl diphosphate (IDP), are

synthesized by two compartmentalized pathways. Both precursor pathways represent interesting targets for biological engineering[13,18-20]. The mevalonate (MEV) pathway converts acetyl-CoA by enzyme activities located in the cytosol, ER and peroxisomes, providing precursors for a wide range of terpenoids with diverse functions such as in growth and development, defense and protein prenylation. The enzyme 3-hydroxy-3-methylglutaryl-CoA reductase (HMGR) catalyzes the rate-limiting step in the MEV pathway and engineering and production of the catalytic domain of HMGR by N-terminal truncation improved the flux of precursors into terpenoid biosynthesis[15,16,21]. Only recently, it was shown that flux through the MEV pathway is, in part, also limited by phosphomevalonate kinase (PMK) which acts downstream of HMGR[22]. The same study provided evidence that isopentenyl diphosphate kinases and hydrolases of the Nudix superfamily are involved in determining the ratio of IDP to isopentenyl phosphate and possibly, the ratios of DMADP to dimethylallyl phosphate and farnesyl diphosphate (FDP) to farnesyl phosphate[22]. Isopentenyl diphosphate kinases reactivate isopentenyl phosphate (IP) through phosphorylation to IDP whereas hydrolases of the Nudix superfamily catalyze the dephosphorylation of IDP.

In the plastid, the 2-*C*-methyl-*D*-erythritol 4-phosphate (MEP) pathway uses pyruvate and *D*-glyceraldehyde 3-phosphate to provide precursors for the biosynthesis of terpenoids related to development, photosynthesis and defense against biotic and abiotic stresses. The enzyme 1-deoxy-*D*-xylulose 5-phosphate synthase (DXS) is rate-limiting in the MEP pathway and its constitutive overproduction enhanced terpenoid production in some, but not all plant species tested[14,23,24]. Head-to-tail condensation of DMADP and IDP affords linear isoprenyl diphosphates, such as FDP (C15) or geranylgeranyl diphosphate (GGDP, C20) catalyzed by farnesyl diphosphate synthase (FDPS) and geranylgeranyl diphosphate synthase (GGDPS), respectively. In *Nicotiana benthamiana*, both DXS and GGDPS were required to enhance terpenoid synthesis[24]. Cytosolic sesquiterpene synthases and plastidial diterpene synthases convert FDPS and GGDPS, respectively, into typically cyclic terpenoid scaffolds,

contributing to the enormous structural diversity among terpenoids in the plant kingdom. Such terpenoid scaffolds often undergo further stereo- and regio-selective functionalization catalyzed by ER membrane-bound mono-oxygenases, cytochromes P450 (CYPs), requiring electrons provided by co-localized NADPH-dependent cytochrome P450 reductases (CPRs).

Despite inherent advantages, such as (native) compartments and availability of reduction equivalents in form of NADPH, terpenoid biotechnology in photosynthetic tissues has remained challenging, as the engineered pathways have to compete for precursors with highly networked native pathways (and their associated regulatory mechanisms). In the present study, we establish methods towards the high-yield production of target terpenoids in leaves co-engineered for triacylglycerol accumulation in lipid droplets in the transient *N. benthamiana* system. Enhanced precursor flux and targeting of terpenoid synthesis enzymes to native and non-native compartments increase terpenoid production. We demonstrate that the lipid droplets sequester produced terpenoids and are suitable organelles to anchor terpenoid biosynthesis steps. By fusing terpenoid enzymes to a microalgal lipid droplet surface protein, terpenoid production is successfully re-targeted to lipid droplets. Our findings will have implications for future generation of stably transformed biomass crops efficiently producing industrially relevant terpenoids in photosynthetic tissues.

RESULTS

Engineered triacylglycerol accumulation

*No*LDSP, a lipid droplet surface protein from the microalga *Nannochloropsis oceanica*, has functions partially analogous to plant oleosins[25]. Similar to oleosins, *No*LDSP possesses a hydrophobic central region that likely mediates the anchoring on lipid droplets. To assess the impact of *No*LDSP on *At*WRI1$^{1-397}$-initiated triacylglycerol accumulation, we infiltrated leaves of *N. benthamiana* with *Agrobacterium tumefaciens* suspensions for transient production of *At*WRI1$^{1-397}$ alone or in combination with *No*LDSP

(*At*WRI1$^{1-397}$+*No*LDSP). In leaves producing *At*WRI1$^{1-397}$ or *At*WRI1$^{1-397}$+*No*LDSP, the triacylglycerol level was approximately 3-fold and 12-fold higher, respectively, than in control leaves without *At*WRI1$^{1-397}$ (Figure 1a). The results clearly demonstrated that the microalgal *No*LDSP had no negative impact on triacylglycerol production and enhanced the accumulation of lipid droplets in infiltrated *N. benthamiana* leaves.

Sesquiterpenoid production in the cytosol and plastids

We then tested different engineering strategies for the production of sesquiterpenoids using patchoulol as a model compound. Like many other sesquiterpenoids, patchoulol is volatile and its engineered production in transgenic lines of *N. tabacum* resulted in significant losses from volatile emission[15]. In our study, losses by atmospheric terpenoid emission were not recorded as the engineering strategies were designed to sequester target terpenoids in lipid droplets in the plant biomass. Transient production of cytosolic *Pogostemon cablin* patchoulol synthase (cytosol:*Pc*PAS) led to formation of a single low-level product, patchoulol, which was not detected in wild-type control plants (Figure 1b). To enhance the precursor availability for sesquiterpenoid synthesis, a feedback-insensitive form of *Euphorbia lathyris* HMGR (*El*HMGR$^{159-582}$) and *A. thaliana* FDPS (cytosol:*At*FDPS) were included in the transient assays. *E. lathyris* accumulates high levels of triterpenoids and their esters[26], suggesting that its HMGR could be a robust enzyme for sesquiterpenoid production in *N. benthamiana*. The selection of the *A. thaliana* FDPS was based on its relatively high thermal stability[27]. The patchoulol content in *N. benthamiana* leaves producing *El*HMGR$^{159-582}$+cytosol:*At*FDPS+cytosol:*Pc*PAS was approximately 5-fold higher than in leaves with cytosol:*Pc*PAS which is consistent with enhanced precursor flux. Co-engineering of patchoulol and triacylglycerol synthesis impaired cytosolic terpenoid accumulation, independent of whether precursor availability was increased or not (Figure 1b).

A previous study demonstrated that re-direction of *Pc*PAS and avian FDPS to the plastid increased the (retained) patchoulol level in leaves of stable transgenic *N. tabacum* lines up to approximately 30 μg patchoulol g^{-1} fresh weight[15]. We modified this approach to further examine engineering strategies for the co-production of patchoulol and lipid droplets in *N. benthamiana* leaves. Targeting of patchoulol synthase to the plastids (plastid:*Pc*PAS) led to accumulation of approximately 0.5 μg patchoulol g^{-1} fresh weight (Figure 1c). To increase the precursor flux in the plastids, *P. barbatus* DXS (*Pb*DXS) and plastid-targeted *At*FDPS (plastid:*At*FDPS) were combined with plastid:*Pc*PAS in the assays. This strategy resulted in a 60-fold increase in the level of patchoulol (Figure 1c). Synthetic lipid droplet accumulation impaired patchoulol production in leaves in the absence of *Pb*DXS and plastid:*At*FDPS, when precursor synthesis was not co-engineered (Figure 1c). The negative impact of lipid droplet production on patchoulol synthesis was rescued when plastid:*At*FDPS or *Pb*DXS+plastid:*At*FDPS were included in the assay. Leaves transiently producing *Pb*DXS+plastid:*At*FDPS+plastid:*Pc*PAS+*At*WRI1$^{1-397}$+*No*LDSP yielded the highest patchoulol level retained in leaves (up to approximately 45 μg patchoulol g^{-1} fresh weight), an average 90-fold and 1.5-fold higher compared to leaves producing plastid:*Pc*PAS and *Pb*DXS+plastid:*At*FDPS+plastid:*Pc*PAS, respectively.

Diterpenoid scaffold production in plastids and cytosol

Strategies for diterpenoid production in the *N. benthamiana* system were examined using the *Abies grandis* abietadiene synthase (*Ag*ABS) as diterpene synthase[28,29]. The bifunctional enzyme has class II and class I terpene synthase activity and catalyzes both the bicyclization of GGDP to a (+)-copalyl diphosphate intermediate and the subsequent secondary cyclization and further rearrangement. Transient production of the native plastidial *A. grandis* abietadiene synthase (plastid:*Ag*ABS) resulted in the accumulation of abietadiene (abieta-7,13-diene), levopimaradiene (abieta-8(14),12-diene), neoabietadiene (abieta-8(14),13(15)-diene) and, as minor product, palustradiene (abieta-8,13-diene)

consistent with the previous findings[30]. These diterpenoids were not detected in wild-type control leaves of *N. benthamiana*. Sole production of plastid:*Ag*ABS yielded approximately 40 μg diterpenoids g^{-1} fresh weight (Figure 2a). To enhance the production of diterpenoids, plastid:*Ag*ABS was co-produced in different combinations with *Pb*DXS and a plastid GGDPS. GGDPSs are differentiated into three types (type I-III) according to their amino acid sequences around the first aspartate-rich motif. These three types differ in their mechanism of determining product chain-length[31,32]. Plant GGDPSs are type II enzymes that are regulated on gene expression, transcript and protein level[33-35]. We hypothesized that inclusion of distantly related type I and type III GGDPSs or a cyanobacterial type II GGDPS may allow us to bypass potential regulatory steps limiting diterpenoid production in *N. benthamiana*. Six GGDPSs were selected: an archaeal GGDPS from *Sulfolobus acidocaldarius* (*Sa*GGDPS, type I), a predicted archaeal GGDPS from *Methanothermobacter thermautotrophicus* (*Mt*GGDPS, type I), a predicted cyanobacterial GGDPS from *Tolypothrix* sp. PCC 7601 (*Ts*GGDPS, type II), two predicted plant GGDPSs from *Euphorbia peplus* (*Ep*GGDPS1 and *Ep*GGDPS2, type II), and one predicted GGDPS from the fungus *Mortierella elongata* AG77 (*Me*GGDPS, type III). *Sa*GGDPS, *Mt*GGDPS, and *Me*GGDPS share only 24%, 25% and 17% amino acid identities with *Ep*GGDPS1, respectively, whereas *Ts*GGDPS and *Ep*GGDPS2 share 48% and 58% identities with *Ep*GGDPS1, respectively. For transient assays in *N. benthamiana*, the coding sequences for the bacterial and fungal GGDPSs were codon-optimized (except for *Ts*GGDPS) and modified to target the enzymes to the plastids, referred to as plastid:*Sa*GGDPS, plastid:*Mt*GGDPS, plastid:*Ts*GGDPS and plastid:*Me*GGDPS. Co-production of *Pb*DXS+plastid:*Ag*ABS or plastid:GGDPS+plastid:*Ag*ABS was insufficient to increase the diterpenoid content in *N. benthamiana* leaves more than 2-fold compared to the diterpenoid level in plastid:*Ag*ABS-producing leaves (Figure 2a). In contrast, co-production of *Pb*DXS+GGDPS+plastid:*Ag*ABS enhanced diterpenoid production up to 6.5-fold compared to leaves producing plastid:*Ag*ABS). Significant differences in diterpenoid yields were obtained depending on which GGDPS was included, apparently unrelated to a specific type of GGDPS

(Figure 2a). The highest diterpenoid levels were determined in *N. benthamiana* leaves co-producing *Pb*DXS+plastid:*Ag*ABS with plastid:*Mt*GGDPS (type I), plastid:*Ts*GGDPS (type II), or *Ep*GGDPS2 (type II), with similar yield between these combinations (Figure 2a).

We further evaluated diterpenoid accumulation in the presence of lipid droplets. Co-production of plastid:*Ag*ABS+*At*WRI1$^{1-397}$ had no significant impact on the diterpenoid level compared to control leaves producing plastid:*Ag*ABS, whereas in leaves producing plastid:*Ag*ABS+*At*WRI1$^{1-397}$+*No*LDSP, the diterpenoid content was increased 2-fold (Figure 2b). Similarly, co-production of plastid:*Mt*GGDPS+ plastid:*Ag*ABS+*At*WRI1$^{1-397}$+*No*LDSP increased the diterpenoid level 2.5-fold compared to plastid:*Mt*GGDPS+plastid:*Ag*ABS producing leaves. The results indicated that the increased abundance of lipid droplets was beneficial for the accumulation of diterpenoid products. Sequestration of the lipophilic diterpenoids into lipid droplets may have helped to circumvent negative feedback regulatory mechanisms and served as "pull force" in diterpenoid production. In fact, isolated lipid droplet fractions from leaves producing plastid:*Ag*ABS+*At*WRI1$^{1-397}$ and plastid:*Ag*ABS+*At*WRI1$^{1-397}$+*No*LDSP contained approximately 35-fold and 460-fold more diterpenoids, respectively, than control fractions from leaves with plastid:*Ag*ABS, consistent with the sequestration of diterpenoids in lipid droplets (Supplementary Figure 1). Co-production of *Pb*DXS and plastid:*Mt*GGDPS together with plastid:*Ag*ABS yielded the highest diterpenoid level (Figure 2b) independent of whether *At*WRI1$^{1-397}$ was included for lipid droplet synthesis. In contrast, co-production of *Pb*DXS+plastid:*Mt*GGDPS+plastid:*Ag*ABS together with *At*WRI1$^{1-397}$+*No*LDSP resulted in a significant reduction of the diterpenoid level (compared to leaves producing *Pb*DXS+plastid:*Mt*GGDPS+plastid:*Ag*ABS).

When *A. grandis* abietadiene synthase was targeted to the cytosol (cytosol:*Ag*ABS$^{85-868}$), leaves accumulated approximately 0.2 μg diterpenoids g^{-1} fresh weight and addition of precursor pathway genes enhanced diterpenoid synthesis (Figure 2c). Co-production of cytosol:*Ag*ABS$^{85-868}$ together with *El*HMGR$^{159-582}$ and cytosolic *M. thermautotrophicus* GGDPS (cytosol:*Mt*GGDPS) increased the diterpenoid

yield more than 400-fold (relative to cytosol:*Ag*ABS$^{85-868}$ containing leaves) and, thus, close to the highest diterpenoid yield achieved with plastid engineering approaches (Figures 2c and 2b). Moreover, our data indicated an enhancing effect of lipid droplet accumulation on terpenoid production when cytosol:*Ag*ABS$^{85-868}$ was co-produced with *At*WRI1$^{1-397}$ or *At*WRI1$^{1-397}$+*No*LDSP (Figure 2c). Under these conditions, terpenoid production was increased up to approximately 3-fold which is consistent with diterpenoids being sequestered in lipid droplets. When *El*HMGR$^{159-582}$+cytosol:*Mt*GGDPS+cytosol:*Ag*ABS$^{85-868}$+*At*WRI1$^{1-397}$+*No*LDSP were co-produced, no additive effects of lipid droplet engineering on terpenoid yield were detected (relative to *El*HMGR$^{159-582}$+cytosol:*Mt*GGDPS+cytosol:*Ag*ABS$^{85-868}$) (Figure 2c).

Triacylglycerol analysis of *N. benthamiana* leaves

To examine a potential impact of terpenoid engineering on triacylglycerol yield, the established approaches for low- or high-yield terpenoid synthesis combined with lipid droplet production were further tested. Four days after infiltration, the leaves were subjected to triacylglycerol analysis. Leaves co-engineered for lipid droplet and patchoulol production in the cytosol contained approximately 50% less triacylglycerol than leaves producing *At*WRI1$^{1-397}$+*No*LDSP (Figure 3a). A significant decrease in the triacylglycerol level was also detected when leaves were engineered for cytosol-targeted high-yield production of diterpenoids (compared to leaves producing *At*WRI1$^{1-397}$+*No*LDSP) (Figure 3b). When lipid droplet production was combined with a plastid-targeted approach for high-yield terpenoid synthesis, no negative impact on triacylglycerol accumulation was observed compared to control plants (Figures 3a and 3b).

Targeting diterpenoid production to lipid droplets

We next investigated whether lipid droplets in the cytosol can be used as platform to anchor biosynthetic pathways for the production of functionalized diterpenoids. The proof-of-concept experiments included modified *A. grandis* abietadiene synthase and *Picea sitchensis* cytochrome P450 (*Ps*CYP720B4), previously reported to convert abietadiene and several isomers to the corresponding diterpene resin acids[36]. To target terpenoid synthesis to the lipid droplets, *A. grandis* abietadiene synthase lacking the N-terminal plastid targeting sequence (cytosol:*Ag*ABS$^{85\text{-}868)}$ and truncated *Ps*CYP720B4 lacking the N-terminal membrane-binding domain (cytosol:*Ps*CYP720B4$^{30\text{-}483}$) were produced as C-terminal and N-terminal *No*LDSP-fusion protein, respectively. The *No*LDSP-fusion proteins are here referred to as LD:*Ag*ABS$^{85\text{-}868}$ and LD*:Ps*CYP720B4$^{30\text{-}483}$. The construction of LD:*Ag*ABS$^{85\text{-}868}$ as C-terminal *No*LDSP-fusion protein was inspired by studies reporting on functional, C-terminal tagged diterpene synthases[37,38]. To re-target *Ps*CYP720B4 to lipid droplets (LD:PsCYP720B4$^{30\text{-}483}$), the predicted N-terminal hydrophobic domain of native *Ps*CYP720B4 was replaced by *No*LDSP as a recent publication described that modifications or deletion of the membrane anchoring domain of CYP720B4 did not impair the enzyme's activity[38]. Inclusion of CPRs has been shown to be crucial to drive metabolic fluxes in CYP-mediated production of high-value target compounds in non-native hosts and synthetic compartments[39,40]. In our experiments, *Camptotheca acuminata* CPR (cytosol:*Ca*CPR$^{70\text{-}708}$) was included as *No*LDSP-fusion protein to co-localize the *Ca*CPR and *Ps*CYP720B4 activities on lipid droplets and facilitate the CYP-catalyzed production of functionalized terpenoids. As the C-terminus of CPRs is pivotal for catalytic activity and not suitable for modifications[41,42], the predicted N-terminal hydrophobic domain of native *Ca*CPR was replaced by *No*LDSP to produce the fusion protein LD:*Ca*CPR$^{70\text{-}708}$.

To determine the localization *in planta*, the *No*LDSP-fusion proteins were each produced as yellow fluorescent protein (YFP)-tagged proteins together with *At*WRI1$^{1\text{-}397}$ for lipid droplet production. The YFP-signals in infiltrated leaves were subsequently compared to the signals obtained for YFP-tagged *No*LDSP which indicated that all three YFP-tagged *No*LDSP-fusion proteins were targeted to the surface

of the lipid droplets (Figure 4). It is noteworthy that production of the YFP-tagged *No*LDSP and *No*LDSP-fusion proteins promoted clustering of small lipid droplets *in planta* and in isolated lipid droplet fractions, consistent with a previous report on ectopic production of *A. thaliana* OLEOSIN1 fused to green fluorescent protein[43] (Figure 4, Supplementary Figure 1). As confirmed for *No*LDSP, the clustering of small lipid droplets was independent of the presence or absence of the YFP-tag (Supplementary Figure 2).

To compare different engineering approaches, the *A. grandis* abietadiene synthase was produced as plastid:*Ag*ABS (native), cytosol:*Ag*ABS$^{85\text{-}868}$ or LD:*Ag*ABS$^{85\text{-}868}$, each alone and combined with ER:*Ps*CYP720B4 (native), cytosol:*Ps*CYP720B4$^{30\text{-}483}$ or LD:*Ps*CYP720B4$^{30\text{-}483}$+LD:*Ca*CPR$^{70\text{-}708}$ (Figure 5). Note that these assays also included either *Pb*DXS+plastid:*Mt*GGDPS or *El*HMGR$^{159\text{-}582}$+cytosol:*Mt*GGDPS to increase the precursor flux, and *At*WRI1$^{1\text{-}397}$ to initiate lipid droplet accumulation. *No*LDSP was included in those assays that lacked any *No*LDSP-fusion proteins. Compared to the assays with plastid:*Ag*ABS, production of cytosol:*Ag*ABS$^{85\text{-}868}$ and LD:*Ag*ABS$^{85\text{-}868}$ resulted in similar diterpenoid yield. When native or modified *A. grandis* abietadiene synthase was co-produced with native or modified *P. sitchensis* *Ps*CYP720B4, the leaves accumulated diterpene resin acids in free and glycosylated forms (Supplementary Figures 3-5). The glycosyl modifications of the diterpenoid acids were consistent with those previously reported for engineered terpenoid products and are likely the result of intrinsic defense/detoxification mechanisms in *N. benthamiana*[24,44,45]. Incubation of such leaf extracts with Viscozyme® L resulted in the hydrolysis of the glycosylated diterpenoid acids to free diterpenoid resin acids which allowed determining the level of total diterpenoid acids produced in infiltrated leaves. To compare the different engineering strategies, the levels of both diterpenoids and total diterpenoid acids were quantified for each infiltrated leaf (Figure 5). Co-production of plastid:*Ag*ABS with ER:*Ps*CYP720B4, cytosol:*Ps*CYP720B4$^{30\text{-}483}$ or LD:*Ps*CYP720B4$^{30\text{-}483}$ decreased the diterpenoid level (compared to controls with plastid:*Ag*ABS) and resulted in the accumulation of diterpenoid acids, consistent with diterpenoids

being converted to diterpenoid acids. The level of diterpenoid acids was approximately 4-fold and 3-fold higher in transient assays with plastid:*Ag*ABS including ER:*Ps*CYP720B4 and plastid:*Ag*ABS+LD:*Ps*CYP720B4$^{30-483}$+LD:*Ca*CPR$^{70-708}$ compared to assays including cytosol:*Ps*CYP720B4$^{30-483}$. The highest diterpenoid acid yield in transient assays with cytosol:*Ag*ABS$^{85-868}$ was achieved in combination with ER:*Ps*CYP720B4 which was approximately 2- and 3-fold higher than with cytosol:*Ag*ABS$^{85-868}$ and LD:*Ps*CYP720B4$^{30-483}$+LD:*Ca*CPR$^{70-708}$, respectively (Figure 5). In transient assays with LD:*Ag*ABS$^{85-868}$, the diterpenoid acid level was 2-fold higher in assays with ER:*Ps*CYP720B4 than in assays with either cytosol:*Ps*CYP720B4$^{30-483}$ or LD:*Ps*CYP720B4$^{30-483}$+LD:*Ca*CPR$^{70-708}$ (Figure 5).

DISCUSSION

Our results demonstrate high-yield synthesis of target di- and sesquiterpenoids in engineered lipid droplet-accumulating leaves of *N. benthamiana* when precursor availability is enhanced. The flux of precursors into terpenoid synthesis was increased through co-production of de-regulated, robust enzymes from the MEP or MEV pathway (*Pb*DXS or *El*HMGR$^{159-582}$) and GGDPS or FDPS in the same compartment. The data are consistent with previous studies in *N. benthamiana* reporting on the engineered production of diterpenoids (plastid-targeted) and a sesquiterpenoid (cytosol-targeted)[15,24,38]. Our comparative study with distinct GGDPSs indicates that a type I enzyme such as *Mt*GGDPS can be a robust alternative to type II GGDPS to increase precursor availability for diterpenoid synthesis and circumvent potential negative feedback (Figure 2a and 2b). In principle, this approach can also be applied to optimize FDPS-dependent sesqui- or triterpenoid pathways.

Highest accumulation of the target sesquiterpenoid was achieved in this study through compartmentation of the biosynthetic pathway in the plastid instead of the cytosol (Figure 1c). Diterpenoid production was targeted to the plastid (*Pb*DXS+plastid:*Mt*GGDPS+plastid:AgABS), cytosol or

lipid droplets (*El*HMGR$^{159-582}$+cytosol:*Mt*GGDPS+ cytosol: *Ag*ABS$^{85-868}$/LD:*Ag*ABS$^{85-868}$) with similar success, yielding a high content of target diterpenoids in vegetative tissue. The anchoring of terpenoid biosynthesis enzymes on cytosolic lipid droplets in this study represents a promising approach in terpenoid biotechnology. It bears the potential to spatially re-arrange enzymes, bringing them into closer proximity and create multi-enzyme assemblies. The technology benefits from *No*LDSP's ability to a) anchor fusion proteins on the lipid droplet surface, b) stabilize small lipid droplets with relatively large surface-to-volume ratio and c) promote the clustering of small lipid droplets, thereby creating a large compartment-like structure (Figure 4). Our results demonstrate that both diterpene synthase and CYP were catalytically active at lipid droplets (Figure 5). Notably, the co-production of plastid:*Ag*ABS with either native *Ps*CYP720B4 (ER:*Ps*CYP720B4) or LD*:Ps*CYP720B4$^{30-483}$ resulted in similar diterpenoid acid yields. Targeting of the diterpene synthase to the cytosol or lipid-droplets impaired the production of diterpenoid acids at lipid droplets catalyzed by LD*:Ps*CYP720B4$^{30-483}$ (compared to ER:*Ps*CYP720B4). At this point, it remains unclear if the high-yield production of diterpenoids in the cytosol and their sequestration in the lipid droplets may have interfered with the functionality of the lipid-droplet targeted enzymes whereas plastid-targeting of the diterpene synthase may have resulted in a more favorable distribution of the diterpenoids between plastid, ER and lipid droplets under the selected experimental conditions. Overall, the top terpenoid yields in this study consolidate the versatility of the transient *N. benthamiana* system as a platform to produce terpenoids and test drive terpenoid biotechnology for later production at industrial scales in economically relevant biomass crops. In this context, it must be noted that stable transgenic *N. benthamiana* engineered for plastid-targeted sesquiterpenoid production (plastid:FDPS+plastid:sesquiterpene synthase) exhibited shorter stature, chlorosis of the lower leaves and vein clearing, probably as a result of carbon competition between the engineered and essential native terpenoid pathways[15]. In high biomass crops, the use of inducible or

weaker promoters (instead of strong constitutive promoters) in terpenoid engineering approaches may, therefore, help to prevent or reduce any interference with plant growth and development.

Co-engineering of lipid droplet synthesis in leaves influenced the target terpenoid yield to different extents depending on the applied engineering approach. Production of the diterpene synthase alone or together with GGDPS in the plastid or cytosol combined with high-yield lipid droplet synthesis (*At*WRI1$^{1-397}$+*No*LDSP) enhanced the target diterpenoid yield up to 2.5-fold (Figures 2b and 2c). Under these conditions, diterpenoids were sequestered in synthetic lipid droplets (Supplementary Figure 1), which may have limited negative feedback and enhanced flux towards diterpenoid production. The abundance of engineered lipid droplets may potentially facilitate downstream processes to extract terpenoids from plant material through "trapping" of the target compounds in the oil fraction. The findings are consistent with a recent publication reporting that co-engineering of sesquiterpenoid and lipid droplet production increased the yields of cytosol-derived volatile sesquiterpenoids by 2- to 4-fold[46]. In our study, production of the sesquiterpene synthase alone or together with FDPS combined with high-yield lipid droplet production did, however, not increase the sesquiterpenoid yield (Figures 1b and 1c) suggesting that a certain ratio of sesquiterpenoids to lipid droplets may be critical to retain highly volatile sesquiterpenoids in the cytosol. Recently, an oleosin-based strategy in the plastid was successful to synthesize squalene, a triterpenoid, in plastids and to trap it in plastid lipid droplets[47]. The latter approach may be also suitable to trap plastid-derived volatile terpenoids in vegetative tissues.

When the plastid-targeted high-yield diterpenoid approach was combined with high-yield lipid droplet production, the diterpenoid yield significantly decreased and a trend towards a lower triacylglycerol level was determined (Figures 2b and 3b). Co-engineering of the cytosol-targeted high-yield diterpenoid approach together with high-yield lipid droplet production did not affect the diterpenoid yield but resulted in a significantly lower triacylglycerol yield. The combination of the set of genes for high-yield sesquiterpenoid production with high-yield lipid droplet production negatively

impacted the cytosol-derived sesquiterpenoid yield and resulted in an approximately 50% lower triacylglycerol yield (Figures 1b and 3a) whereas the plastid-derived sesquiterpenoid yield was enhanced without triacylglycerol production being affected. In the plastids of engineered leaves, fatty acid synthesis (initiated by *At*WRI1$^{1-397}$) and terpenoid synthesis likely competed directly for carbon (probably in form of pyruvate), resulting in an increase in the product yield from one pathway at the expense of the other pathway. Although both MEV pathway in the cytosol and fatty acid biosynthesis in the plastid require acetyl-CoA as precursor, a direct competition between these two pathways for acetyl-CoA appears implausible since acetyl-CoA is impermeable to membranes and independently produced and consumed in the different subcellular compartments and organelles of plant cells[48]. As metabolic interactions between the cytosol and plastid are not well understood, it remains unclear whether shifts in cytosolic metabolite pools may have influenced carbon partitioning between the cytosol and plastid.

METHODS

Constructs for transient expression studies

The open reading frames encoding truncated *A. thaliana* WRINKLED1 (*At*WRI1$^{1-397}$, AY254038.2 [https://www.ncbi.nlm.nih.gov/nuccore/AY254038.2/]) and full-length *N. oceanica* lipid droplet surface protein (*No*LDSP, JQ268559.1[https://www.ncbi.nlm.nih.gov/nuccore/JQ268559.1]) were amplified from existing cDNAs[11,25]. The coding sequences for truncated cytosolic *E. lathyris* HMGR (*El*HMGR$^{159-582}$, JQ694150.1[https://www.ncbi.nlm.nih.gov/nuccore/JQ694150.1]), cytosolic *A. thaliana* FDPS (cytosol:*At*FDPS, NM_117823.4[https://www.ncbi.nlm.nih.gov/nuccore/NM_117823.4]), cytosolic *P. cablin* patchoulol synthase (cytosol:*Pc*PAS, AY508730 [https://www.ncbi.nlm.nih.gov/nuccore/AY508730]), plastidic *A. grandis* abietadiene synthase (plastid:*Ag*ABS, U50768.1[https://www.ncbi.nlm.nih.gov/nuccore/U50768.1]), and plastidic *P. barbatus* (*Pb*DXS) were amplified from cDNAs derived from total RNA of the host organisms. The cDNA sequence

for *Pb*DXS used in this study significantly differed from the previously published sequence[38] and was deposited in GenBank. The endoplasmic *P. sitchensis* CYP720B4 (ER:*Ps*CYP720B4, HM245403.1[https://www.ncbi.nlm.nih.gov/nuccore/HM245403.1]) was amplified from a cDNA clone. The open reading frame encoding a truncated *C. acuminata* CPR (*Ca*CPR$^{70\text{-}708}$, KP162177[https://www.ncbi.nlm.nih.gov/nuccore/KP162177]) lacking the N-terminal membrane anchor domain was synthesized. Codon optimized open reading frames were synthesized for the type I GGDPSs from *S. acidocaldarius* (*Sa*GGDPS, D28748.1[https://www.ncbi.nlm.nih.gov/nuccore/D28748.1]) and *M. thermautotrophicus* (*Mt*GGDPS, AE000666.1[https://www.ncbi.nlm.nih.gov/nuccore/AE000666.1]) (Supplementary Data 1). A putative *M. elongata* AG77 *Me*GGDPS (type III) was identified through mining of transcriptome data[49] and a codon optimized open reading frame was synthesized (Supplementary Data 1). Two putative type II GGDPSs, *Ep*GGDPS1 and *Ep*GGDPS2, were identified through mining of *E. peplus* transcriptome data[50] and amplified from leaf cDNA. A putative type II GGDPS was identified in the genome of *Tolypothrix* sp. PCC 7601 (*Ts*GGDPS)[51] and the coding sequence was amplified from genomic DNA. To target *Sa*GGDPS, *Mt*GGDPS, *Ts*GGDPS, *Me*GGDPS, *At*FDPS and *Pc*PAS to the plastid, the sequences were fused at their N-terminus to the plastid targeting sequence of the *A. thaliana* ribulose bisphosphate carboxylase small chain 1A (NM_105379.4[https://www.ncbi.nlm.nih.gov/nuccore/NM_105379.4]). The encoded plastid-targeted proteins are referred to as plastid:*Sa*GGDPS, plastid:*Mt*GGDPS, plastid:*Ts*GGDPS plastid:*Me*GGDPS, plastid:*At*FDPS and plastid:*Pc*PAS. The coding sequences of *A. grandis* abietadiene synthase and *P. sitchensis* CYP720B4 (ER:*Ps*CYP720B4) were truncated to target the enzymes to the cytosol, in this study referred to as cytosol:*Ag*ABS$^{85\text{-}868}$ and cytosol:*Ps*CYP720B4$^{30\text{-}483}$, respectively. For lipid droplet targeting, truncated *A. grandis* abietadiene synthase, *P. sitchensis* CYP720B4 and *C. acuminata* CPR were either fused to the N-terminus or C-terminus of *N. oceanica* lipid droplet surface protein resulting in LD:*Ag*ABS$^{85\text{-}868}$, LD:*Ps*CYP720B4$^{30\text{-}483}$ and LD:*Ca*CPR$^{70\text{-}708}$, respectively (Figure 4). All primers used in this

study are described in Supplementary Table 1. The full-length and modified coding sequences were verified by sequencing, inserted into pENTR4 (Invitrogen), and subsequently transferred into the Gateway vectors pEarleygate 100 and pEarleygate 104 (N-terminal YFP-tag), each under control of a 35S promoter for strong constitutive expression[52]. These constructs were introduced into *A. tumefaciens* LBA4404 for transient expression studies in *N. benthamiana*. Primers and constructs used in the study were designed with SnapGene 3.3.4.

Transient expression in *N. benthamiana* leaves

Transformants of *A. tumefaciens* LBA4404 carrying selected binary vectors were grown overnight at 28°C in Luria-Bertani medium containing 50 µg/mL rifampicin and 50 µg/mL kanamycin. Prior to infiltration into *N. benthamiana* leaves, the *A. tumefaciens* cells were sedimented by centrifugation at 3800 x g for 10 min, washed, resuspended in infiltration buffer (10 mM MES-KOH pH 5.7, 10 mM $MgCl_2$, 200 µM acetosyringone) to an optical density at 600 nm (OD600) 0.8 and incubated for approximately 30 min at 30°C. To test various gene combinations, equal volumes of the selected bacterial suspensions were mixed and infiltrated into *N. benthamiana* leaves using a syringe without a needle. *A. tumefaciens* LBA4404 carrying the tomato bushy stunt virus gene P19[53,54] was included in all infiltrations to suppress RNA silencing in *N. benthamiana*. The *N. benthamiana* plants used for infiltration were grown for 3.5 to 4 weeks in soil at 25°C under a 12-h photoperiod at 150 µmol m^{-2} s^{-1}. To compare different engineering strategies, only plants of the same batch were used in transient assays. Typically, three to five plants were used for each gene combination. To avoid developmental differences, the same two leaves were infiltrated on each plant. After infiltration, the plants were grown for 4 additional days in the growth chamber. Samples from the infiltrated leaves were subsequently analyzed for terpenoid or

419 triacylglycerol content. All experiments were conducted at least two times and the results are shown
420 from representative experiments.
421
422 **Lipid Analysis**
423 Triacylglycerol analyses were performed essentially as previously described with minor
424 modifications[4]. For each sample, one infiltrated *N. benthamiana* leaf was freshly harvested and total
425 lipids were extracted with 4 mL chloroform/methanol/formic acid (10:20:1, by volume). Ten microgram
426 tri-17:0 triacylglycerol (Sigma) was added as internal standard to each sample. The total lipids were
427 separated by thin layer chromatography on silica plates (Si250PA, Mallinckrodt Baker) developed with
428 ether:ethyl ether:acetic acid (80:20:1, v/v/v). Triacylglycerol bands were visualized with a spraying dye
429 (0.01% Primuline in 80% (v/v) acetone) under UV light. The TAG bands were scraped from the TLC plates
430 and used to prepare fatty acid methyl esters by acid-catalyzed trans-methylation in 1 mL 1 M
431 hydrochloric acid in anhydrous methanol at 80°C for 25 min. The samples were extracted with 1 mL
432 0.9% sodium chloride and 1 mL hexane. After centrifugation at 1,000 x g for 3 min, the hexane extract
433 was collected, the volume was reduced under a stream of nitrogen and the extract was subjected to gas-
434 liquid chromatography. Chromatography was performed with an Agilent DB-23 column at 48.6 mL min^{-1}
435 helium flow, 21.93 psi pressure and 250°C inlet temperature. The following oven program was used: 2
436 min isothermal at 140°C, 25°C min^{-1} to 160°C, 8°C min^{-1} to 250°C, 4 min isothermal at 250°C followed by
437 38°C min^{-1} to 140°C. The temperature of the flame ionization detector was 270°C with 30.0 mL min^{-1}
438 hydrogen flow, 400 mL min^{-1} air flow and 30.0 mL min^{-1} helium flow. All triacylglycerol analysis was
439 performed in Excel 2010.
440 **Statistical Analyses**

441 Statistical analyses were conducted using Graphpad Prism 8 and included normality (Shapiro-Wilk),
442 one-way ANOVA (Welch and Brown-Forsythe) and *t*-tests (unpaired, two-tailed, Welch correction). A *P*-
443 value of <0.05 was considered statistically significant.
444
445 **Terpenoid analyses in *N. benthamiana* leaves**
446 For each sample, 50 mg or 100 mg leaf tissue was incubated with 1 mL hexane containing 2 mg mL^{-1}
447 1-eicosene (internal standard, TCI America) on a shaker for 15 min at room temperature prior to
448 incubation in the dark for 16 h at room temperature. Sesquiterpenoids and diterpenoids were separated
449 and analyzed by GC-MS using an Agilent 7890A GC system coupled to an Agilent 5975C MS detector.
450 Chromatography was performed with an Agilent VF-5ms column (40 m $\times$ 0.25 mm $\times$ 0.25 μm) at 1.2 mL
451 min^{-1} helium flow. The injection volume was 1 μL in splitless mode at an injector temperature of 250°C.
452 The following oven program was used (run time 18.74 min): 1 min isothermal at 40°C, 40°C min^{-1} to
453 180°C, 2 min isothermal at 180°C, 15°C min^{-1} to 300°C, 1 min isothermal at 300°C, 100°C min^{-1} to 325°C
454 and 3 min isothermal at 325°C. The mass spectrometer was operated at 70 eV electron ionization mode,
455 a solvent delay of 3 min, ion source temperature at 230°C, and quadrupole temperature at 150°C. Mass
456 spectra were recorded from m/z 30 to 600. Terpenoid products were identified based on retention
457 times, mass spectra published in relevant literature and through comparison with the NIST Mass
458 Spectral Library v17 (National Institute of Standards and Technology, USA). Quantitation of diterpenoid
459 products and patchoulol was based on 1-eicosene standard curves. The extracted ion chromatograms
460 for each target compound were integrated, and compounds were quantified using QuanLynx tool
461 (Waters) with a mass window allowance of 0.2 and a signal-to-noise ratio ≥10. All calculated peak areas
462 were normalized to the peak area for the internal standard 1-eicosene and tissue fresh weight.

463 Diterpenoid resin acids and glycosylated derivatives were analyzed by UHPLC/MS/MS to confirm
464 accurate masses and fragments. For each sample, 100 mg leaf tissue and 1 mL methanol containing
465 1.25 μM telmisartan (internal standard, Toronto Research Chemicals) were added, mixed and incubated
466 in the dark at room temperature for 16 h. A 10-μL volume of each extract was subsequently analyzed
467 using a 31-min gradient elution method on an Acquity BEH C18 UHPLC column (2.1 × 100 mm, 1.7 μm,
468 Waters) with mobile phases consisting of 0.15% formic acid in water (solvent A) and acetonitrile (solvent
469 B). The 31-min method gradient employed 1% B at 0.00 to 1 min, linear gradient to 99% B at 28.00 min,
470 held until 30 min, followed by a return to 1% B and held from 30.10 to 31 min. The flow rate was 0.3
471 mL/min and the column temperature was 40°C. The mass spectrometer (Xevo G2-XS QTOF, Waters) was
472 equipped with an electrospray ionization source and operated in negative-ion mode. Source parameters
473 were as follows: capillary voltage 2500 V, cone voltage 40 V, desolvation temperature 300°C, source
474 temperature 100°C, cone gas flow 50 L/h, and desolvation gas flow 600 L/h. Mass spectrum acquisition
475 was performed in negative ion mode over m/z 50 to 1500 with scan time of 0.2 s using a collision energy
476 ramp 20 to 80 V. For quantitative analyses of the total diterpenoid resin acid level, 50 mg leaf tissue was
477 incubated with 1 mL methanol/water (8/2, v/v) containing 2 μM telmisartan (internal standard, Toronto
478 Research Chemicals) in the dark at room temperature. Note that a second sample was taken from each
479 infiltrated leaf and subjected to diterpenoid analysis as described above. After 16 h, 200-μL aliquots of
480 the methanol/water extracts were dried down under vacuum, reconstituted in 500 μL McIlvaine buffer
481 (citrate phosphate buffer) pH 4.0 and incubated with 100 μL Viscozyme® L (Sigma Aldrich) at 37°C for
482 16 h. Viscozyme® L is a multi-enzyme complex with a wide range of carbohydrase activities. After
483 overnight incubation, samples were extracted with 500 μL dichloromethane, centrifuged for 10 min at
484 4,000 g, 250-μL aliquots were then transferred to fresh glass vials, dried down under vacuum and
485 resuspended in 50 μL 80% (v/v) methanol. A 10-μL volume of each extract was subsequently analyzed by

UHPLC/MS/MS using a 16-min gradient elution method with mobile phases consisting of 10 mM ammonium formate in water (solvent A) and methanol (solvent B). The 16-min method gradient employed 20% B at 0.00 to 2 min, linear gradient to 99% B at 14.00 min, held until 15 min, followed by a return to 20% B and held from 15.10 to 16 min. The mass spectrometer was operated in negative-ion mode. MassLynx v4.1 was used for acquisition and processing of GC-MS and UHPLC/MS/MS data.

Isolation of lipid droplets

Lipid droplets were isolated as previously described with minor adjustments[55]. For each sample, 1 g infiltrated *N. benthamiana* leaf tissue was ground with mortar and pestle in 20 mL ice-cold buffer A (20 mM tricine, 250 mM sucrose, 0.2 mM phenylmethylsulfonyl fluoride pH 7.8). The homogenate was filtered through Miracloth (Calbiochem) and centrifuged in a 50-mL tube at 3,400 g for 10 min at 4°C to remove cell debris. From each tube, 10 mL supernatant was collected and transferred to a 15-mL tube. The supernatant fraction was then overlaid with 3 mL buffer B (20 mM HEPES, 100 mM KCl, 2 mM $MgCl_2$, pH 7.4) and centrifuged for 1 h at 5,000 g. After centrifugation, 2 mL from the top of each gradient containing floating lipid droplets were collected. For terpenoid analysis, each lipid droplet fraction was extracted with 5 mL hexane containing 2 μg mL^{-1} 1-eicosene (internal standard, TCI America) prior to GC-MS analysis. To avoid developmental differences, the same leaf from three different plants (biological replicates) were analyzed for each gene combination.

Confocal imaging

For lipid droplet visualization, sections of freshly harvested leaf samples were stained on microscope slides with Nile red solution (10 μg mL^{-1} in phosphate buffered saline) in the dark. After one hour, the sections were briefly rinsed with phosphate buffered saline prior to microscopy. Imaging of Nile red, chlorophyll and enhanced yellow fluorescent protein (EYFP) fluorescence was conducted with a

confocal laser scanning microscope FluoView VF1000 (Olympus) at excitation 559 nm/emission 570-630 nm, excitation 559 nm/emission 655-755 nm and excitation 515 nm/emission 527 nm, respectively. Images were processed using the FV10-ASW 4.2 microscopy software (Olympus).

DATA AVAILABILITY

Sequence data from this article were newly deposited in the GenBank/EMBL data libraries under the following accession numbers: MH363711[https://www.ncbi.nlm.nih.gov/nuccore/MH363711] (*EpGGDPS1*), MH363712[https://www.ncbi.nlm.nih.gov/nuccore/MH363712] (*EpGGDPS2*), MH363713[https://www.ncbi.nlm.nih.gov/nuccore/MH363713] (*PbDXS*) and MH363714[https://www.ncbi.nlm.nih.gov/nuccore/MH363714] (*TsGGDPS*). The codon optimized sequences for *SaGGDPS*, *MtGGDPS* and *MeGGDPS* are given in Supplementary Data 1. The source data underlying Figs. 1, 2, 3 and 5 and Supplementary Figure 1b are provided as a Source Data file.

COMPETING INTERESTS

RS, CB and BH are inventors on a provisional patent application at Michigan State University covering the findings discussed. PK, JC, YY and AB declare no competing interests.

ACKNOWLEDGMENTS

We thank Beronda Montgomery (Michigan State University) for the *Tolypothrix* sp. PCC 7601 cells, Jörg Bohlmann (University of British Columbia, Canada) for the *Ps*CYP720B4 cDNA, and Afton M. Dewyse, Robert Nolan, Jonathan A. Arnesen, Britta Hamberger and Emily Lockwood at Michigan State University for technical assistance. We extend our thanks to Melinda Frame at the Center for Advanced Microscopy (Michigan State University) and A. Dan Jones and Tony Schilmiller at Michigan State University for assistance in the identification of the glycosylated diterpenoid acids. Mass spectra were

collected using instruments at the Michigan State University Mass Spectrometry and Metabolomics core. This work was primarily supported by the U.S. Department of Energy-Great Lakes Bioenergy Research Center Cooperative Agreement DE-FC02-07ER64494 (BH, CB) and partially by the Division of Chemical Sciences, Geosciences and Biosciences, Office of Basic Energy Sciences of the U.S. Department of Energy Grant DE- DE-FG02-91ER20021 (CB) and by AgBioResearch MICL02357 (CB), Michigan State University. BH gratefully acknowledges startup funding from the Department of Molecular Biology and Biochemistry, AgBioResearch (MICL02454) and the U.S. Department of Energy Grant (DE-SC0018409), Michigan State University.

AUTHOR CONTRIBUTIONS

R.S. designed the study and performed the experiments, analyzed the data and wrote the article; R.S., P.K., J.C. and A.B. generated expression constructs, and Y.Y. performed triacylglycerol analysis. C.B. and B.H. conceived the study and edited the drafts of the article.

REFERENCES

1 Chapman, K. D. & Ohlrogge, J. B. Compartmentation of triacylglycerol accumulation in plants. *J. Biol. Chem.* **287**, 2288-2294 (2012).

2 Li, M. *et al.* Purification and structural characterization of the central hydrophobic domain of oleosin. *J. Biol. Chem.* **277**, 37888-37895 (2002).

3 Zale, J. *et al.* Metabolic engineering of sugarcane to accumulate energy-dense triacylglycerols in vegetative biomass. *Plant Biotechnol. J.* **14**, 661-669 (2016).

4 Yang, Y. *et al.* Ectopic expression of *WRI1* affects fatty acid homeostasis in *Brachypodium distachyon* vegetative tissues. *Plant Physiol.* **169**,1836-1847 (2015).

5 Du, Z. Y. & Benning, C. Triacylglycerol accumulation in photosynthetic cells in plants and algae. *Subcell. Biochem.* **86**, 179-205 (2016).

6 Cernac, A. & Benning, C. *WRINKLED1* encodes an AP2/EREB domain protein involved in the control of storage compound biosynthesis in Arabidopsis. *Plant J.* **40**, 575-585 (2004).

7 Maeo, K. *et al.* An AP2-type transcription factor, WRINKLED1, of *Arabidopsis thaliana* binds to the AW-box sequence conserved among proximal upstream regions of genes involved in fatty acid synthesis. *Plant J.* **60**, 476-487 (2009).

8 Sanjaya, Durrett, T. P., Weise, S. E. & Benning, C. Increasing the energy density of vegetative tissues by diverting carbon from starch to oil biosynthesis in transgenic Arabidopsis. *Plant Biotechnol. J.* **9**, 874-883 (2011).

9 Vanhercke, T. *et al.* Metabolic engineering of biomass for high energy density: oilseed-like triacylglycerol yields from plant leaves. *Plant Biotechnol. J.* **12**, 231-239 (2014).

10 Grimberg, A., Carlsson, A. S., Marttila, S., Bhalerao, R. & Hofvander, P. Transcriptional transitions in *Nicotiana benthamiana* leaves upon induction of oil synthesis by WRINKLED1 homologs from diverse species and tissues. *BMC Plant Biol.* **15**, 192 (2015).

11 Ma, W. *et al.* Deletion of a C-terminal intrinsically disordered region of WRINKLED1 affects its stability and enhances oil accumulation in Arabidopsis. *Plant J.* **83**, 864-874 (2015).

12 Lange, B. M. & Ahkami, A. Metabolic engineering of plant monoterpenes, sesquiterpenes and diterpenes-current status and future opportunities. *Plant Biotechnol. J.* **11**, 169-196 (2013).

13 Augustin, J. M., Higashi, Y., Feng, X. & Kutchan, T. M. Production of mono- and sesquiterpenes in *Camelina sativa* oilseed. *Planta* **242**, 693-708 (2015).

14 Reed, J. *et al.* A translational synthetic biology platform for rapid access to gram-scale quantities of novel drug-like molecules. *Metab. Eng.* **42**, 185-193 (2017).

15 Wu, S. *et al.* Redirection of cytosolic or plastidic isoprenoid precursors elevates terpene production in plants. *Nat. Biotechnol.* **24**, 1441-1447 (2006).

16 Lange, B.M. The evolution of plant secretory structures and emergence of terpenoid chemical diversity. Annu. Rev. Plant Biol. **66**, 139-159 (2015).

17 Pateraki, I. *et al.* Manoyl oxide (13R), the biosynthetic precursor of forskolin, is synthesized in specialized root cork cells in *Coleus forskohlii*. *Plant Physiol.* **164**, 1222-1236 (2014).

18 Liao, P., Hemmerlin, A., Bach, T. J. & Chye, M. L. The potential of the mevalonate pathway for enhanced isoprenoid production. *Biotechnol. Adv.* **34**, 697-713 (2016).

19 Frank, A. & Groll, M. The Methylerythritol Phosphate Pathway to Isoprenoids. *Chem. Rev.* **117**, 5675-5703 (2017).

20 Banerjee, A. & Sharkey, T. D. Methylerythritol 4-phosphate (MEP) pathway metabolic regulation. *Nat. Prod. Rep.* **31**, 1043-1055 (2014).

21 Chappell, J., Wolf, F., Proulx, J., Cuellar, R. & Saunders, C. Is the reaction catalyzed by 3-hydroxy-3-methylglutaryl coenzyme A reductase a rate-limiting step for isoprenoid biosynthesis in plants? *Plant Physiol.* **109**, 1337-1343 (1995).

22 Henry, L.K., Thomas, S.T., Widhalm, J.R., Lynch, J.H., Davis, T.C., Kessler, S.A., Bohlmann, J., Noel, J.P., Dudareva, N. Contribution of isopentenyl phosphate to plant terpenoid metabolism. Nat. Plants **4**, 721-729 (2018).

23 Estevez, J. M., Cantero, A., Reindl, A., Reichler, S. & Leon, P. 1-Deoxy-D-xylulose-5-phosphate synthase, a limiting enzyme for plastidic isoprenoid biosynthesis in plants. *J. Biol. Chem.* **276**, 22901-22909 (2001).

24 Bruckner, K. & Tissier, A. High-level diterpene production by transient expression in *Nicotiana benthamiana*. *Plant Methods* **9**, 46 (2013).

25 Vieler, A., Brubaker, S. B., Vick, B. & Benning, C. A lipid droplet protein of *Nannochloropsis* with functions partially analogous to plant oleosins. *Plant Physiol.* **158**, 1562-1569 (2012).

26 Skrukrud, C. L., Taylor, S. E., Hawkins, D. R. & Calvin, M. in *The Metabolism, Structure, and Function of Plant Lipids* (eds. Paul K. Stumpf, J. Brian Mudd, & W. David Nes) 115-118 (Springer New York, 1987).

27 Keim, V. *et al.* Characterization of Arabidopsis FPS isozymes and FPS gene expression analysis provide insight into the biosynthesis of isoprenoid precursors in seeds. *PloS One* **7**, e49109 (2012).

28 Vogel, B. S., Wildung, M. R., Vogel, G. & Croteau, R. Abietadiene synthase from grand fir (*Abies grandis*): cDNA isolation, characterization, and bacterial expression of a bifunctional diterpene cyclase involved in resin acid biosynthesis. *J. Biol. Chem.* **271**, 23262-23268 (1996).

29 Peters, R. J. *et al.* Abietadiene synthase from grand fir (*Abies grandis*): characterization and mechanism of action of the "pseudomature" recombinant enzyme. *Biochem.* **39**, 15592-15602 (2000).

30 Keeling, C. I., Madilao, L. L., Zerbe, P., Dullat, H. K. & Bohlmann, J. The primary diterpene synthase products of *Picea abies* levopimaradiene/abietadiene synthase (PaLAS) are epimers of a thermally unstable diterpenol. *J. Biol. Chem.* **286**, 21145-21153 (2011).

31 Noike, M., Katagiri, T., Nakayama, T., Nishino, T. & Hemmi, H. Effect of mutagenesis at the region upstream from the G(Q/E) motif of three types of geranylgeranyl diphosphate synthase on product chain-length. *J. Biosci. Bioeng.* **107**, 235-239 (2009).

32 Chang, T. H., Guo, R. T., Ko, T. P., Wang, A. H. & Liang, P. H. Crystal structure of type-III geranylgeranyl pyrophosphate synthase from *Saccharomyces cerevisiae* and the mechanism of product chain length determination. *J. Biol. Chem.* **281**, 14991-15000 (2006).

33 Xu, Q. *et al.* Discovery and comparative profiling of microRNAs in a sweet orange red-flesh mutant and its wild type. *BMC Genomics* **11**, 246-246 (2010).

34 Zhou, F. *et al.* A recruiting protein of geranylgeranyl diphosphate synthase controls metabolic flux toward chlorophyll biosynthesis in rice. *Proc. Natl. Acad. Sci.* **114**, 6866-6871 (2017).

35 Ruiz-Sola, M. A. *et al.* Arabidopsis GERANYLGERANYL DIPHOSPHATE SYNTHASE 11 is a hub isozyme required for the production of most photosynthesis-related isoprenoids. *New Phytol.* **209**, 252-264 (2016).

36 Hamberger, B., Ohnishi, T., Hamberger, B., Seguin, A. & Bohlmann, J. Evolution of diterpene metabolism: Sitka spruce CYP720B4 catalyzes multiple oxidations in resin acid biosynthesis of conifer defense against insects. *Plant Physiol.* **157**, 1677-1695 (2011).

37 Yahyaa, M., Matsuba, Y., Brandt, W., Doron-Faigenboim, A., Bar, E., McClain, A.,Davidovich-Rikanati, R., Lewinsohn, E., Pichersky, E., Ibdah, M. Identification, Functional Characterization, and Evolution of Terpene Synthases from a Basal Dicot. Plant Physiol. **169**, 1683-1697 (2015).

38 Gnanasekaran, T. *et al.* Heterologous expression of the isopimaric acid pathway in *Nicotiana benthamiana* and the effect of N-terminal modifications of the involved cytochrome P450 enzyme. *J. Biol. Eng.* **9**, 24 (2015).

39 Renault, H., Bassard, J.E., Hamberger, B., Werck-Reichhart, D. Cytochrome P450-mediated metabolic engineering: current progress and future challenges. Curr. Opin. Plant Biol. **19**, 27-34 (2014).

40 Bavishi, K., Laursen, T., Martinez, K.L., Møller, B.L., Della Pia, E.A. Application of nanodisc technology for direct electrochemical investigation of plant cytochrome P450s and their NADPH P450 oxidoreductase. Sci. Rep. 6, 29459 (2016).

41 Qu, X., Pu, X., Chen, F., Yang, Y., Yang, L., Zhang, G., Luo, Y. Molecular Cloning, Heterologous Expression, and Functional Characterization of an NADPH-Cytochrome P450 Reductase Gene from *Camptotheca acuminata*, a Camptothecin-Producing Plant. PLoS One **10**, e0135397 (2015).

42 Qu, X., Pu, X., Chen, F., Yang, Y., Yang, L., Zhang, G., Luo, Y. Correction: Molecular Cloning, Heterologous Expression, and Functional Characterization of an NADPH-Cytochrome P450 Reductase Gene from *Camptotheca acuminata*, a Camptothecin-Producing Plant. PLoS One **10**, e0139647 (2015).

43 Fan, J., Yan, C., Zhang, X. & Xu, C. Dual role for phospholipid:diacylglycerol acyltransferase: enhancing fatty acid synthesis and diverting fatty acids from membrane lipids to triacylglycerol in Arabidopsis leaves. *Plant Cell* **25**, 3506-3518 (2013).

44 Dong, L., Jongedijk, E., Bouwmeester, H. & Van Der Krol, A. Monoterpene biosynthesis potential of plant subcellular compartments. *New Phytol.* **209**, 679-690 (2016).

45 van Herpen, T. W. *et al. Nicotiana benthamiana* as a production platform for artemisinin precursors. *PloS One* **5**, e14222 (2010).

46 Delatte, T. L. *et al.* Engineering storage capacity for volatile sesquiterpenes in *Nicotiana benthamiana* leaves. *Plant Biotechnol. J.* **16**, 1997-2006 (2018).

47 Zhao, C. *et al.* Co-Compartmentation of terpene biosynthesis and storage via synthetic droplet. *ACS Synth. Biol.* **7**,774-781 (2018).

48 Oliver, D.J., Nikolau, B.J. & Wurtele, E.S. Acetyl-CoA - Life at the metabolic nexus. *Plant Sci.* **176**, 597-601 (2009).

49 Uehling, J. *et al.* Comparative genomics of *Mortierella elongata* and its bacterial endosymbiont *Mycoavidus cysteinexigens*. *Environ. Microbiol.* **19**, 2964-2983 (2017).

50 Xiao, M. *et al.* Transcriptome analysis based on next-generation sequencing of non-model plants producing specialized metabolites of biotechnological interest. *J. Biotechnol.* **166**, 122-134 (2013).

51 Yerrapragada, S. *et al.* Extreme sensory complexity encoded in the 10-megabase draft genome sequence of the chromatically acclimating cyanobacterium *Tolypothrix* sp. PCC 7601. *Genome Announc.* **3**, e00355-15 (2015).

52 Earley, K. W. *et al.* Gateway-compatible vectors for plant functional genomics and proteomics. *Plant J.* **45**, 616-629 (2006).

53 Voinnet, O., Pinto, Y. M. & Baulcombe, D. C. Suppression of gene silencing: a general strategy used by diverse DNA and RNA viruses of plants. *Proc. Natl. Acad. Sci.* **96**, 14147-14152 (1999).

54 Voinnet, O., Pinto, Y. M. & Baulcombe, D. C. Correction for Voinnet et al., Suppression of gene silencing: A general strategy used by diverse DNA and RNA viruses of plants. *Proc. Natl. Acad. Sci.* **112**, E4812 (2015).

55 Ding, Y. *et al.* Isolating lipid droplets from multiple species. *Nat. Protoc.* **8**, 43 (2012).

FIGURE LEGENDS

Figure 1. Engineered patchoulol production in *N. benthamiana* leaves. Triacylglycerol (TAG) accumulation was initiated through expression of *WRINKLED1* (*AtWRI1*$^{1\text{-}397}$) and further enhanced through co-expression of *No*LDSP (**a**). Patchoulol production was engineered in the cytosol (**b**) and in the plastid (**c**) in the absence and presence of *At*WRI1$^{1\text{-}397}$ and *No*LDSP. To enhance FDP availability for patchoulol production, *El*HMGR$^{159\text{-}582}$ (cytosol), *Pb*DXS (plastid) and *At*FDPS (cytosol, plastid) were included in transient assays. The different construct combinations are indicated below each bar (black

694 circle, was included; minus, was not included) and in the scheme next to each graph. Data were
695 analyzed by Shapiro-Wilk, Welch-ANOVA (**a**, *P* 0.0006; **b**, *P*<0.0001; **c**, *P*<0.0001) and Brown-Forsythe
696 ANOVA (**a**, *P* 0.0004; **b**, *P*<0.0001; **c**, *P*<0.0001) followed by *t*-tests (unpaired, two-tailed, Welch
697 correction). Data are presented as individual biological replicates and bars representing average levels
698 with SD (**a**, *N*=4; **b**, *N* indicated below each bar*;* **c**, *N*=8). This experiment was replicated twice.
699 Statistically significant differences are indicated by ***a-e*** based on *t*-tests (*P*<0.05). Source Data are
700 provided as a Source Data file. LD, lipid droplet

701

702 **Figure 2. Engineered diterpenoid production in *N. benthamiana* leaves.** Production of *Ag*ABS led to
703 accumulation of diterpenoids (abietadiene and its isomers). To enhance GGDP availability for
704 diterpenoid production, *El*HMGR$^{159\text{-}582}$ (cytosol), *Pb*DXS (plastid) and distinct GGDPSs (cytosol or plastid)
705 were included in transient assays. The protein combinations are indicated below each bar (black circle,
706 was included; minus, was not included) and in the scheme next to each graph. The production of
707 diterpenoids was engineered in the plastid (**a**, **b**) and in the cytosol (**c**) in the absence and presence of
708 *At*WRI1$^{1\text{-}397}$ and *No*LDSP. Data were analyzed by Shapiro-Wilk, Welch-ANOVA (**a**, *P*<0.0001; **b**, *P*<0.0001;
709 **c**, *P*<0.0001) and Brown-Forsythe ANOVA (**a**, *P*<0.0001; **b**, *P*<0.0001; **c**, *P*<0.0001) followed by *t*-tests
710 (unpaired, two-tailed, Welch correction). Data are presented as individual biological replicates and bars
711 representing average levels with SD (*N* indicated below each bar). This experiment was replicated twice.
712 Statistically significant differences are indicated by ***a-e*** based on *t*-tests (*P*<0.05). Source Data are
713 provided as a Source Data file. LD, lipid droplet

714

715 **Figure 3. Triacylglycerol yield in engineered *N. benthamiana* leaves.** TAG accumulation was initiated
716 through ectopic expression of *WRINKLED1* (*AtWRI1*$^{1\text{-}397}$) and further enhanced through co-expression of

*No*LDSP. The impact of engineered patchoulol (**a**) and diterpenoid production (**b**) on TAG yield is depicted. The different construct combinations are indicated below each bar (black circle, was included; minus, was not included). Data were analyzed by Shapiro-Wilk, Welch-ANOVA (**a**, $P<0.0001$; **b**, $P<0.0001$) and Brown-Forsythe ANOVA (**a**, $P<0.0001$; **b**, $P<0.0001$) followed by *t*-tests (unpaired, two-tailed, Welch correction). Data are presented as individual biological replicates and bars representing average levels with SD (*N* indicated below each bar). This experiment was replicated twice. Statistically significant differences are indicated by *a-e* based on *t*-tests ($P<0.05$). Source Data are provided as a Source Data file.

Figure 4. Localization of heterologously expressed fluorescent-reporter tagged fusion proteins. *N. benthamiana* leaves producing *yellow fluorescent protein* (YFP)-tagged *No*LDSP, LD:*Ag*ABS$^{85-868}$, LD:*Ps*CYP720B4$^{30-483}$ or LD:*Ca*CPR$^{70-708}$ were subjected to confocal laser scanning microscopy. Representative images are shown. The produced YFP-proteins are indicated in each line. Note that *At*WRI1$^{1-397}$ was co-produced and leaf samples were stained with Nile red to visualize neutral lipids in lipid droplets. This experiment was replicated twice. Channels: **YFP**, *yellow fluorescent protein* (scale bar 20 μm); **NR**, Nile red (scale bar 20 μm); **YFP, NR**, enlarged merge YFP and NR (scale bar 5 μm)

Figure 5. Lipid droplets as engineering platform for the production of functionalized diterpenoids. Terpenoid biosynthesis enzymes were produced as *No*LDSP-fusion proteins to target them to the lipid droplets (LD:*Ag*ABS$^{85-868}$, LD:*Ps*CYP720B4$^{430-483}$ and LD:*Ca*CPR$^{70-708}$) and tested in different combinations as indicated below each bar (black circle, was included; minus, was not included) (**a**). Production of native or modified *Ag*ABS led to accumulation of diterpenoids and when native or modified *Ps*CYP720B4 was co-produced, to conversion of diterpenoids to diterpenoid acids. Data were analyzed by Shapiro-

Wilk, Brown-Forsythe ANOVA (diterpenoids *P* 0.0184, *P*<0.0001, *P*<0.0001; diterpenoid acids *P*<0.0001, *P*<0.0001, *P*<0.0001) and Welch ANOVA (diterpenoids *P* 0.0509, *P* 0.0002, *P*<0.0001; diterpenoid acids *P*<0.0001, *P*<0.0001, *P* 0.0002) followed by *t*-tests (unpaired, two-tailed, Welch correction). Results are presented as individual biological replicates and bars representing average levels with SD (*N* indicated below each bar). Statistically significant differences are indicated by *a-d* based on *t*-tests (*P*<0.05). This experiment was replicated twice. The scheme (**b**) depicts the conversion of abietadiene to abietic acid when LD:*Ag*ABS$^{85\text{-}868}$ (*No*LDSP-*Ag*ABS), LD:*Ps*CYP720B4$^{430\text{-}483}$ (*No*LDSP-*Ps*CYP) and LD:*Ca*CPR$^{70\text{-}708}$ (*No*LDSP-*Ca*CPR) were produced. Source Data are provided as a Source Data file. LD, lipid droplet; e^-, electron from NADPH

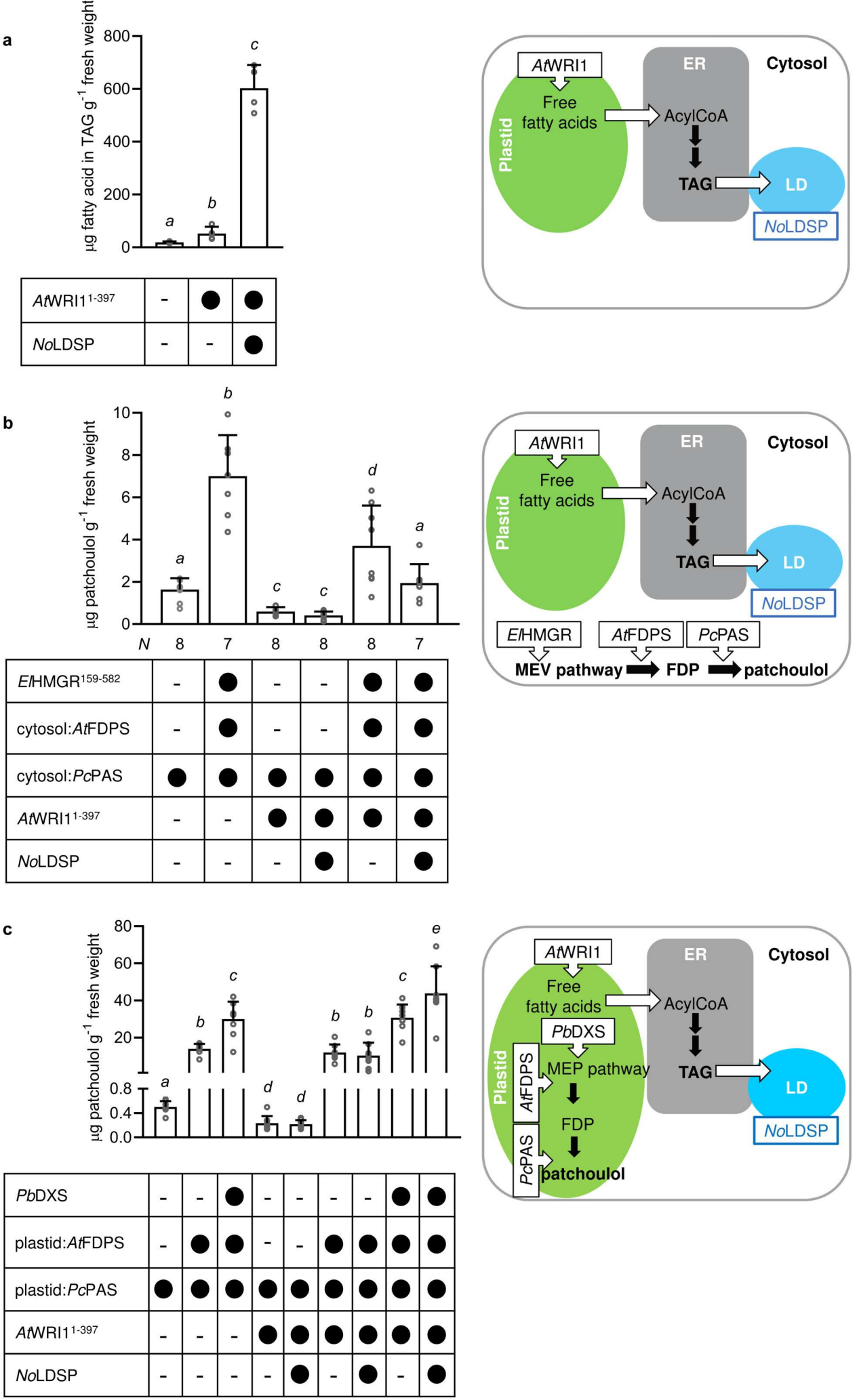
a
µg fatty acid in TAG g-1 fresh weight
800
600
400
200
0
a
b
c
AtWRI1 1-397
NoLDSP
AtWRI1
Free
fatty acids
Plastid
ER
Cytosol
AcylCoA
TAG
LD
NoLDSP
b
µg patchoulol g-1 fresh weight
10
8
6
4
2
0
a
b
c
c
d
a
N
8
7
8
8
8
7
ElHMGR 159-582
cytosol:AtFDPS
cytosol:PcPAS
AtWRI1 1-397
NoLDSP
AtWRI1
Free
fatty acids
Plastid
ER
Cytosol
AcylCoA
TAG
LD
NoLDSP
ElHMGR
AtFDPS
PcPAS
MEV pathway
FDP
patchoulol
c
µg patchoulol g-1 fresh weight
80
60
40
20
0.8
0.4
0.0
a
b
c
d
d
b
b
c
e
PbDXS
plastid:AtFDPS
plastid:PcPAS
AtWRI1 1-397
NoLDSP
AtWRI1
Free
fatty acids
PbDXS
Plastid
AtFDPS
MEP pathway
FDP
PcPAS
patchoulol
ER
Cytosol
AcylCoA
TAG
LD
NoLDSP

a

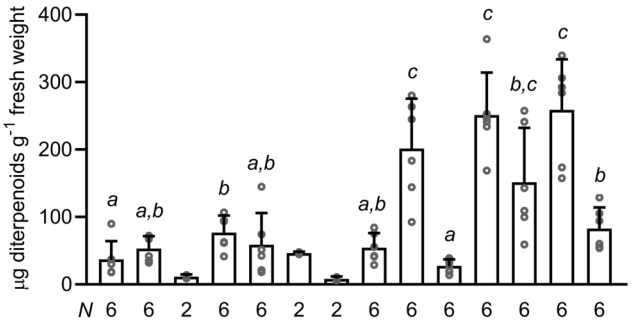

*Pb*DXS	-	-	-	-	-	-	-	●	●	●	●	●	●	●
plastid:*Mt*GGDPS	-	●	-	-	-	-	-	-	●	-	-	-	-	-
plastid:*Sa*GGDPS	-	-	●	-	-	-	-	-	-	●	-	-	-	-
plastid:*Ts*GGDPS	-	-	-	●	-	-	-	-	-	-	●	-	-	-
plastid:*Ep*GGDPS1	-	-	-	-	●	-	-	-	-	-	-	●	-	-
plastid:*Ep*GGDPS2	-	-	-	-	-	●	-	-	-	-	-	-	●	-
plastid:*Me*GGDPS	-	-	-	-	-	-	●	-	-	-	-	-	-	●
plastid:*Ag*ABS	●	●	●	●	●	●	●	●	●	●	●	●	●	●

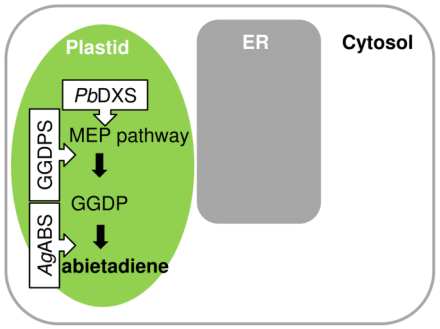

b

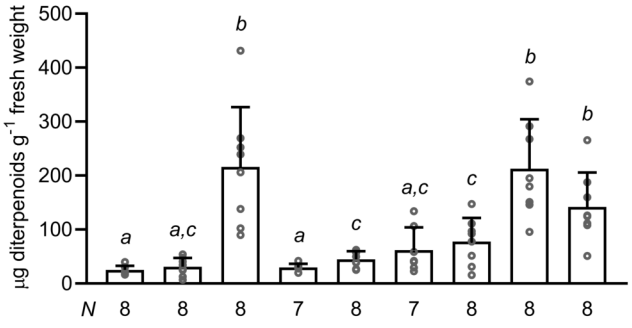

*Pb*DXS	-	-	●	-	-	-	-	●	●
plastid:*Mt*GGDPS	-	●	●	-	-	●	●	●	●
plastid:*Ag*ABS	●	●	●	●	●	●	●	●	●
*At*WRI1$^{1-397}$	-	-	-	●	●	●	●	●	●
*No*LDSP	-	-	-	-	●	-	●	-	●

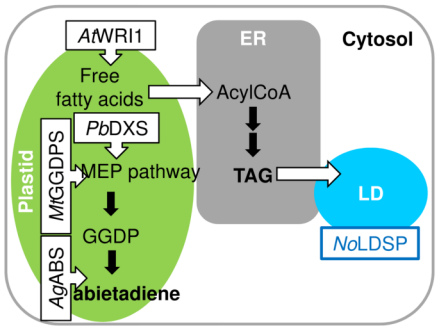

c

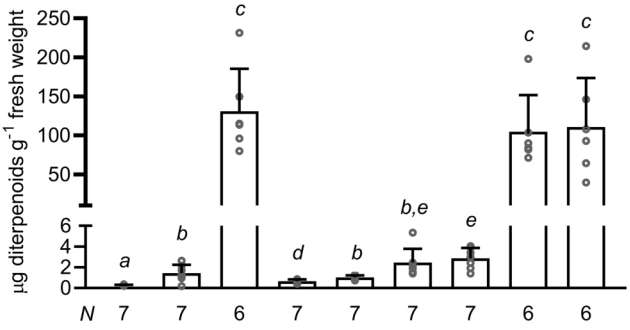

*El*HMGR$^{159-582}$	-	-	●	-	-	-	-	●	●
cytosol:*Mt*GGDPS	-	●	●	-	-	●	●	●	●
cytosol:*Ag*ABS$^{85-868}$	●	●	●	●	●	●	●	●	●
*At*WRI1$^{1-397}$	-	-	-	●	●	●	●	●	●
*No*LDSP	-	-	-	-	●	-	●	-	●

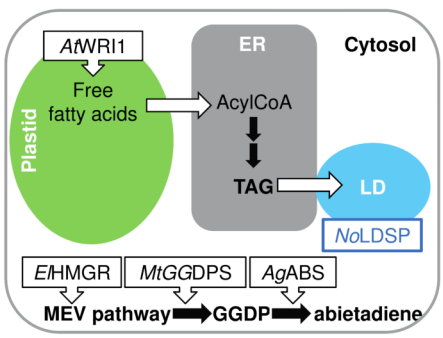

a

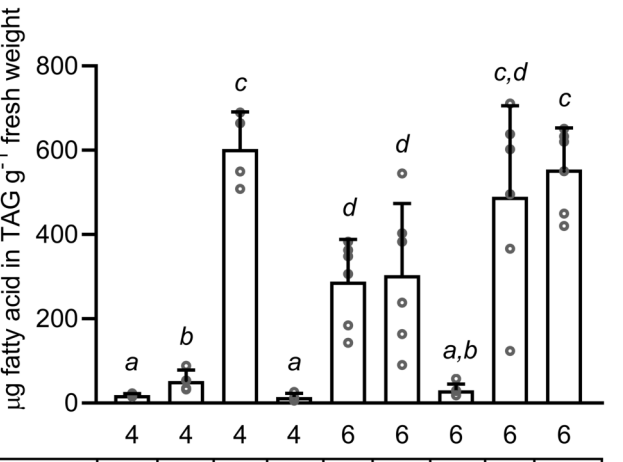

*At*WRI1$^{1-397}$	-	●	●	-	●	●	-	●	●
*No*LDSP	-	-	●	-	●	●	-	●	●
*El*HMGR$^{159-582}$	-	-	-	-	-	●	-	-	-
cytosol:*At*FDPS	-	-	-	-	-	●	-	-	-
cytosol:*Pc*PAS	-	-	-	●	●	●	-	-	-
*Pb*DXS	-	-	-	-	-	-	-	-	●
plastid:*At*FDPS	-	-	-	-	-	-	-	-	●
plastid:*Pc*PAS	-	-	-	-	-	-	●	●	●

b

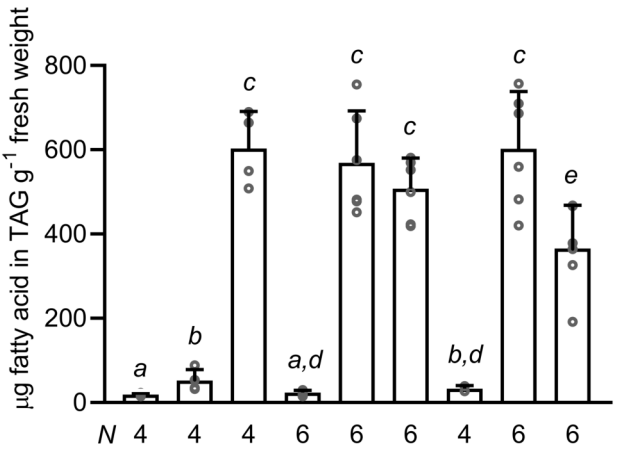

*At*WRI1$^{1-397}$	-	●	●	-	●	●	-	●	●
*No*LDSP	-	-	●	-	●	●	-	●	●
*Pb*DXS	-	-	-	-	-	●	-	-	-
plastid:*Mt*GGDPS	-	-	-	-	-	●	-	-	-
plastid:*Ag*ABS	-	-	-	●	●	●	-	-	-
*El*HMGR$^{159-582}$	-	-	-	-	-	-	-	-	●
cytosol:*Mt*GGDPS	-	-	-	-	-	-	-	-	●
cytosol:*Ag*ABS$^{85-868}$	-	-	-	-	-	-	●	●	●

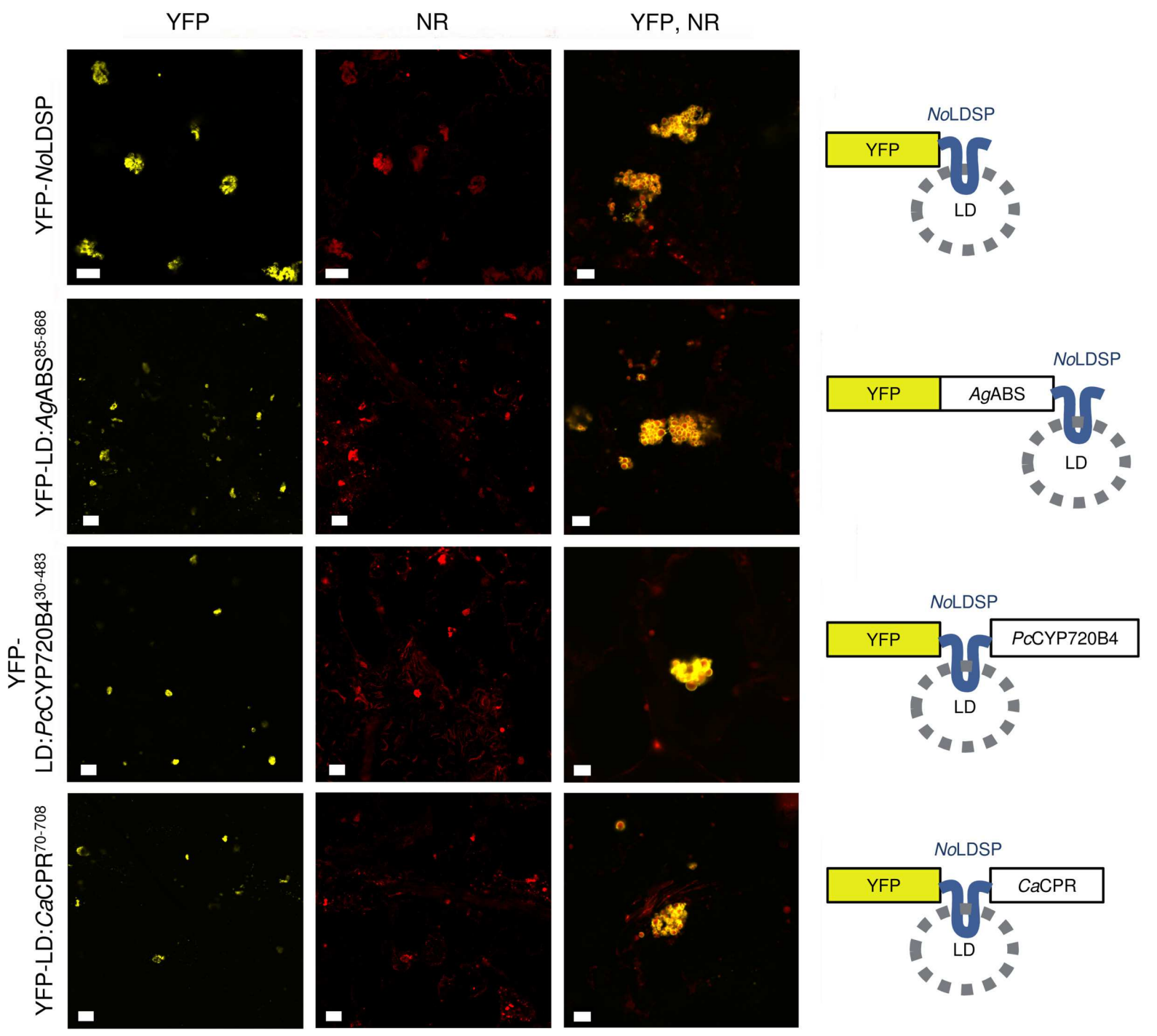
YFP
NR
YFP, NR
YFP-NoLDSP
YFP-LD:AgABS85-868
YFP-LD:PcCYP720B430-483
YFP-LD:CaCPR70-708
NoLDSP
YFP
LD
NoLDSP
YFP
AgABS
LD
NoLDSP
YFP
PcCYP720B4
LD
NoLDSP
YFP
CaCPR
LD

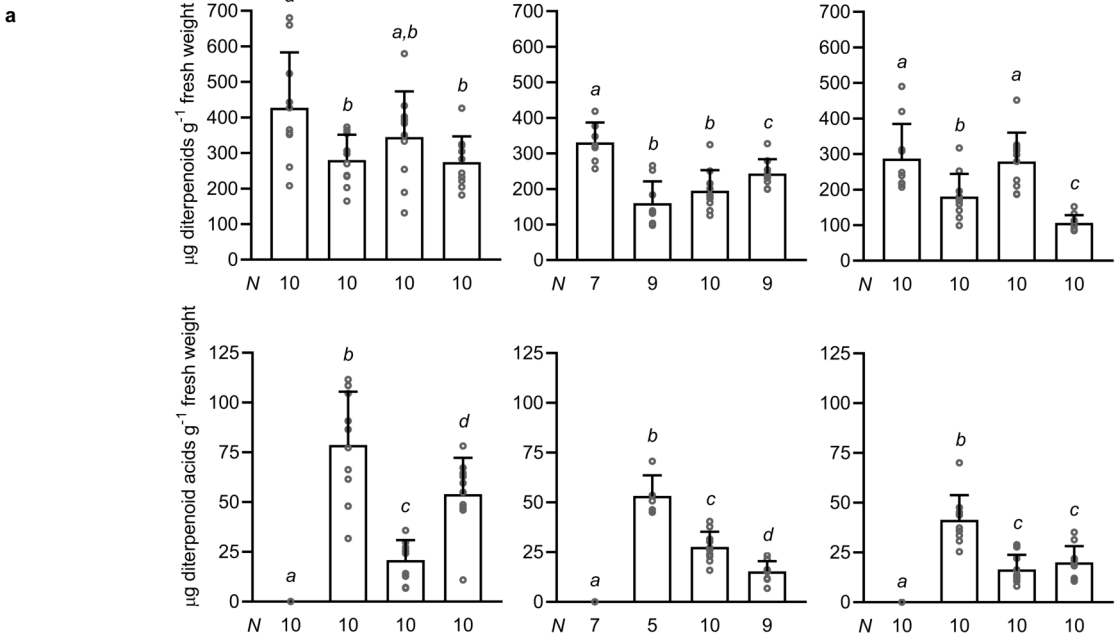

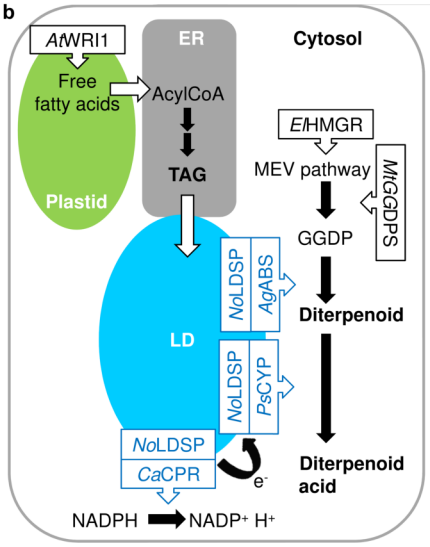

*Pb*DXS	●	●	●	●	-	-	-	-	-	-	-	-
plastid:*Mt*GGDPS	●	●	●	●	-	-	-	-	-	-	-	-
plastid:*Ag*ABS	●	●	●	●	-	-	-	-	-	-	-	-
*Et*HMGR$^{159\text{-}582}$	-	-	-	-	●	●	●	●	●	●	●	●
cytosol:*Mt*GGDPS	-	-	-	-	●	●	●	●	●	●	●	●
cytosol:*Ag*ABS$^{85\text{-}868}$	-	-	-	-	●	●	●	●	-	-	-	-
LD:*Ag*ABS$^{85\text{-}868}$	-	-	-	-	-	-	-	-	●	●	●	●
ER:*Ps*CYP720B4	-	●	-	-	-	●	-	-	-	●	-	-
cytosol:*Ps*CYP720B4$^{30\text{-}483}$	-	-	●	-	-	-	●	-	-	-	●	-
LD:*Ps*CYP720B4$^{30\text{-}483}$	-	-	-	●	-	-	-	●	-	-	-	●
LD:*Ca*CPR$^{70\text{-}708}$	-	-	-	●	-	-	-	●	-	-	-	●
*At*WRI1$^{1\text{-}397}$	●	●	●	●	●	●	●	●	●	●	●	●
*No*LDSP	●	●	●	-	●	●	●	-	●	●	●	-